

Power-grid modelling via gradual improvement of parameters

B. Hartmann,¹ G. Ódor,² K. Benedek,^{2,3} and I. Papp²

¹*Institute of Energy Security and Environmental Safety, HUN-REN Centre for Energy Research, P.O. Box 49, H-1525 Budapest, Hungary*

²*Institute of Technical Physics and Materials Science, HUN-REN Centre for Energy Research, P.O. Box 49, H-1525 Budapest, Hungary*

³*Department of Theoretical Physics, Budapest University of Technology and Economics, Budafoki út 8, H-1111 Budapest, Hungary*

(*Electronic mail: hartmann.balint@ek.hun-ren.hu)

The dynamics of electric power systems are widely studied through the phase synchronization of oscillators, typically with the use of the Kuramoto equation. While there are numerous well-known order parameters to characterize these dynamics, shortcomings of these metrics are also recognized. To capture all transitions from phase disordered states over phase locking to fully synchronized systems, new metrics were proposed and demonstrated on homogeneous models. In this paper we aim to address a gap in the literature, namely, to examine how gradual improvement of power grid models affect the goodness of certain metrics. To study how the details of models are perceived by the different metrics, 12 variations of a power grid model were created, introducing varying level of heterogeneity through the coupling strength, the nodal powers and the moment of inertia. The grid models were compared using a second-order Kuramoto equation and adaptive Runge-Kutta solver, measuring the values of the phase, the frequency and the universal order parameters. Finally, frequency results of the models were compared to grid measurements. We found that the universal order parameter was able to capture more details of the grid models, especially in cases of decreasing moment of inertia. The most heterogeneous models showed very low synchronization and thus suggest a limitation of the second-order Kuramoto equation. Finally, we show local frequency results related to the multi-peaks of static models, which implies that spatial heterogeneity can also induce such multi-peak behaviour.

Modeling power-grid systems has got a major importance in present days as transformation to renewable energy sources requires the complete re-design of energy transmission. Renewable energy sources can be located quite far from their consumption points because urban and industrial structures do not follow physical constraints and capabilities. Important examples are the sea coast vs inland divisions in the case of wind power. Ill-constructed high-voltage (HV) power grids can cause catastrophic damages to economies as it was demonstrated in recent history via the emergence of large blackout events¹⁻⁵. The probability distributions of such events was found to be fat-tailed, exhibiting power-law (PL) tails very often⁶. To understand them, self-organized critical direct current (DC) models have been constructed⁷ and have been shown to describe well the PL exponents of empirical values. However, many details could not be understood as power-grids work with alternating currents (AC) in which phase differences are the primary causes of the power-flows.

can be mitigated by the enhanced fluctuations, that arise naturally in the neighborhood of synchronization transition points, where power grids self-organize themselves by the competition of supply and demand^{9-11,19,20}.

In power grid systems, the focus is often on the phase synchronization of the individual oscillators²¹ since their steady state is usually a stable limit cycle. To study the synchronization dynamics, several order parameters are used to characterize the dynamic state of the system. In the literature, there are numerous well-known Kuramoto order parameters, such as the complex order parameter^{21,22}, the local order parameter measuring the phase coherence and its global variant²³, a mean-field variant of the complex order parameter²⁴ or the one respecting network topology²⁵.

Shortcomings of these metrics have been highlighted in a number of papers, most importantly by Ref. ²⁶, who claim that existing order parameters are not fully suitable to characterize complex oscillator networks as they don't capture all transitions from incoherence over phase locking to full synchrony for arbitrary, finite networks. Hence a universal order parameter was also introduced, which captures partial phase locking, respects the topology of the network, and has been shown to increase monotonically with the coupling strength.

In this paper, we aim to address a research gap in the literature, namely to examine how different modeling assumptions regarding the heterogeneities of a power grid are captured by the different order parameters. In the different scenarios, to analyze and compare the dynamic behavior of the various models, we will use the frequency spread, the global order parameter, and the newly proposed universal order parameter by ref.²⁶ as the main measures. We also present a frequency analysis of the simulation results and confirm q-Gaussian distributions, matching real data distributions presented in one of

I. INTRODUCTION

AC modelling of power-grids have been proposed since the equivalence of swing equations to the second-order Kuramoto model was shown⁸. Failures leading to blackouts have been studied by composite Kuramoto and threshold models² and the PL tailed cascade failures could be modelled by them⁹⁻¹¹. Network topological features, which lead to desynchronization by network fragmentation and Braess paradox phenomena, have been identified¹²⁻¹⁸. We have shown that these are basically consequences of quenched heterogeneity, which

our earlier work²⁰.

The remainder of the paper is structured as follows. Section II introduces the synchronization model and the twelve grid models. Section III presents the results organized around five aspects. Finally, these results are discussed in Section IV, and conclusions are drawn.

II. DATA AND MODELS

A. The synchronization model

Modeling power-grid systems come in different flavors, but at the heart of most approaches describing the time evolution lies the so-called swing equations²⁷, set up for mechanical elements (e.g. rotors in generators and motors) with inertia. Mathematically it is formally equivalent to the second-order Kuramoto equation⁸, for a network of N oscillators with phases $\theta_i(t)$.

To investigate the effects of different parametrizations and to facilitate benchmarking with previous results, we used a more specific form^{9,11,20,28}, which includes dimensionless electrical parametrization and approximations for unknown ones:

$$\ddot{\theta}_i + \alpha \dot{\theta}_i = \frac{P_i}{I_i \omega_S} + \frac{P_i^{max}}{I_i \omega_S} \sum_{j=1}^N W_{ij} \sin(\theta_j - \theta_i) + \Omega_i. \quad (1)$$

In this equation θ_i is the phase angle, $\omega_i = \dot{\theta}_i$, is the frequency of node i , α is the dissipation or damping factor, W_{ij} is the coupling strength and P_i is the source/load power. Furthermore, I_i denotes the rotation inertia, ω_S the system frequency, and P_i^{max} the maximal transmitted power in the system. Note that we can also have an intrinsic frequency of nodes $\Omega_i = 50$ Hz (in Europe), but it can be transformed out in a rotating frame and we have omitted it in the calculations. Our frequency results show the deviations from this value.

If we know more details of the electrical parameters we can cast this into the form with real physical dimensions:

$$\dot{\omega}_i = -\frac{D_i \omega_i}{M_i \omega_S} + \frac{L_i}{M_i \omega_S} + \sum_{j=1}^N \frac{Y_{ij} V_i V_j}{M_i \omega_S} \sin(\theta_j - \theta_i), \quad (2)$$

where D_i has dimension of $\left[\frac{\text{kg} \cdot \text{m}^2}{\text{s}^2} \right]$ and describes the damping effect of element i in the system, $L_i \left[\frac{\text{kg} \cdot \text{m}^2}{\text{s}^3} \right]$ is the power capacity of node i , $Y_{ij} = \frac{1}{X_{ij}} \left[\frac{1}{\Omega} \right]$ is the susceptance of lines, the inverse of reactance, V_i [V] is the nodal voltage level and $M_i \left[\text{kg} \cdot \text{m}^2 \right]$ is the moment of inertia.

Topological heterogeneity of power grids is the result of two factors, (i) the structure and connectivity of the grid itself, and (ii) the heterogeneity of power line capacities and nodal behaviors, as it was presented in our recent work²⁰. In the second-order Kuramoto equation, these varying properties are represented by the parameters L_i , Y_{ij} and M_i .

The time step resolution of the calculations was set to be $\Delta t = 0.25$ s and $\alpha = 0.1$ was used, similarly as in Refs^{29,30}.

Ref.³⁰ also used $\alpha = 0.4$. In this way, the results of the Kuramoto equation become dimensionless.

To model station fluctuations, we have added a multiplicative, quenched noise to the source/sink terms of 2

$$\eta_{i,j} = 0.05 \xi_j \frac{P_i}{I_i \omega_S}, \quad (3)$$

where $\xi_j \in N(0,1)$ is drawn from a zero centered Gaussian distribution. To solve the equations of motion we used an adaptive, Runge-Kutta-4, from the package Numerical Recipes.

We investigated the standard synchronization measures of the phases $R(t)$ and the frequency spread $\Omega(t)$, called the frequency order parameter. We measured the Kuramoto phase order parameter:

$$z(t_k) = r(t_k) \exp[i\theta(t_k)] = 1/N \sum_j \exp[i\theta_j(t_k)]. \quad (4)$$

Sample averages over different initial fluctuations for the phases

$$R(t_k) = \langle r(t_k) \rangle \quad (5)$$

and for the variance of the frequencies

$$\Omega(t_k) = \frac{1}{N} \left\langle \sum_{j=1}^N (\bar{\omega}(t_k) - \omega_j t_k)^2 \right\rangle \quad (6)$$

were determined, where $\bar{\omega}(t_k)$ denotes the mean frequency within each respective sample at time step $t_k = 1 + 1.08^k$, $k = 1, 2, 3, \dots$. Sample averages were computed from the solutions with hundreds of independent self-frequency realizations (i.e. $\eta_{i,j}$) for each control parameter.

Besides, we measured a more complex order parameter suggested for the second-order Kuramoto model, which claimed to accurately track the degree of partial phase locking and synchronization²⁶

$$r_{iui}(t_k) = 1 / \left(\sum_{i,j} w_{ij} \right) \sum_{i,j} w_{ij} \cos(\theta_i - \theta_j) \quad (7)$$

and it's sample and temporal average in the steady state:

$$R_{uni} = \langle r_{iui}(t_k) \rangle \quad (8)$$

The fluctuations of the order parameters are measured by the standard deviations of the sample and temporal averages in the steady state, typically after 100 s transient time.

B. The grid model

We chose the Hungarian high-voltage (132, 220, and 400 kV) network to create our grid models. The network consists of 387 nodes and 640 edges, and its most important features are presented in Table I. Cross-border transmission lines were reduced to their domestic terminals as sources or consumers, thus resulting in a standalone synchronous system. In

TABLE I. Selected characteristics of the Hungarian power grid. N and E denote the number of nodes and edges. $\langle k \rangle$ is the average degree, L is the average shortest path, C is the clustering coefficient, Q is the modularity quotient³¹. σ and ω are small-world metrics according to Fronczak et al.³² and Telesford et al.³³, Eff is the global efficiency of the network³⁴, and γ is the decay exponent of the exponential of the degree distribution³⁵.

| N | E | $\langle k \rangle$ | L | C | Q | σ | ω | Eff | γ |
|-----|-----|---------------------|-------|-------|--------|----------|----------|-------|----------|
| 387 | 640 | 3.307 | 6.566 | 0.077 | 0.4666 | 6.855 | 0.521 | 0.177 | 1.726 |

the modeled loading state, 351 nodes behave as consumers and 36 as sources.

In order to study how modeling depth is perceived by the different order parameters, we created 12 different variations of the Hungarian network. These variations introduce heterogeneity to the parameters W_{ij} , L_i , and M_i . The resulting representations thus range from completely homogeneous networks, which are the most widely covered in related literature, to completely heterogeneous ones, where electric parameters and nodal behaviors are defined using the actual data and measurements of the Hungarian system. The following assumptions are used for the three parameters.

- W_{ij} , coupling strength:
 1. Identical value for each edge, the value corresponding to the largest thermal capacity (ampacity) limit in the system (approx. 1400 MW). This option represents the benchmark used by e.g. Refs.^{29,30}.
 2. Unique value for each edge, depending on their actual thermal capacity limits (range between 40 and 1400 MW).
 3. Unique value for each edge, depending on their actual admittance Y_{ij} and voltage level.
- L_i , nodal power:
 1. The sources ($L_i < 0$) are distributed equally among the nodes representing power plants and the consumers ($L_i > 0$) are distributed equally among nodes truly representing consumption. This is a slightly modified assumption of Ref.³⁰, where half the nodes correspond to consumers ($L_i > 0$), while the other half to power sources ($L_i < 0$).
 2. Every L_i value is uniquely assigned, based on measured data (SCADA).
- M_i , moment of inertia:
 1. Aligning with the literature, we set a constant value for M_i , corresponding to a 400MW gas turbine power plant as in^{29,30}.
 2. We evenly distribute the moment of inertia among 400kV and 220kV nodes, which host the majority of synchronous generators (conventional power plants).

3. We evenly distribute the moment of inertia along all nodes of the model.
4. We set unique values based on measured data and whether the node actually hosts a synchronous machine or not.

In the following the 12 scenarios will refer to the different models as shown in Table II.

TABLE II. The different scenarios, representing increasing level of heterogeneity in modelling. The numbers from the table correspond to the list number of the assumption for the respective parameter.

| Scenario # | 1 | 2 | 3 | 4 | 5 | 6 | 7 | 8 | 9 | 10 | 11 | 12 |
|------------|---|---|---|---|---|---|---|---|---|----|----|----|
| W_{ij} | 1 | 1 | 1 | 1 | 2 | 2 | 2 | 2 | 3 | 3 | 3 | 3 |
| L_i | 1 | 1 | 1 | 2 | 1 | 1 | 1 | 2 | 1 | 1 | 1 | 2 |
| M_i | 1 | 2 | 3 | 4 | 1 | 2 | 3 | 4 | 1 | 2 | 3 | 4 |

III. RESULTS

In the following, results of the synchronization studies are presented in a sequential, interdependent way. First, the coupling strength was varied to compare how different order parameters display criticality (Section III A). Then the transient behaviour of the three order parameters, R , Ω and R_{uni} are analysed in sections III B, III C and III D, respectively. Section III E compares the frequency data of the simulations to grid frequency data presented in Ref.²⁰.

Note that to assist the interpretation of the results, not all scenarios are displayed in all figures.

A. Dependence of the critical point on the models

We assume that power-grid-like systems operate near the state of self-organized criticality (SOC)^{9,36–38}. This means that the system is not operated on 100% load capacity, but usually at a lower level. To mimic the not fully loaded behavior we can cast equation (1) in the following form:

$$\ddot{\theta}_i + \alpha \dot{\theta}_i = \frac{P_i}{I_i \omega_S} + \frac{P_i^{max}}{I_i \omega_S} \lambda \sum_{j=1}^N W_{ij} \sin(\theta_j - \theta_i). \quad (9)$$

The multiplicative factor λ in front of the interaction term is the chosen constant for the system and its value corresponds to different load levels. Alternatively it can be also said, that the initial $\frac{P_i^{max}}{I_i \omega_S}$ term transforms to $\frac{P_i}{I_i \omega_S}$, with arbitrary P_i power. In a mathematical sense this maps to a changing coupling strength, which allows us to identify the SOC behavior by analyzing the standard deviation of the Kuramoto order parameter.

To identify the cross-over point to synchronization (cf. fig. 1), we varied the λ parameter from 0.1 to 1.0 with steps of 0.1. For the sake of completeness, we performed analysis starting the system from a phase-ordered state, i.e. all oscillators have the same initial phase and some noise, or from a disordered

phase, i.e. all the oscillators have random initial phase assignment. In the figures of this section, dash-dotted lines with unfilled markers will represent the phase-ordered states, and continuous lines with filled markers are the disordered states.

We have chosen model scenarios 1, 5, and 9 for finding the optimal λ value, as these scenarios represent homogeneous nodal behavior with three different options for defining the coupling strength. We performed the statistical calculation on a minimum 2500 sample and a maximum 7500 for each λ value. The results are shown in Figs. 1-3 for R , Ω and R_{uni} , respectively.

Fig. 1 shows that the behavior of the phase-ordered curves (dash-dotted lines with unfilled markers) is non-trivial. As the curves of scenarios 1, 5, and 9 overlap, this implies that R does not capture the difference in modeling the coupling strength. Very similar results were obtained for Ω -s, as shown in Fig. 2.

Fig. 3 displays that the R_{uni} order parameter indeed increases monotonically with the exception of the case of scenario 9, phase ordered initial condition, large λ values. Also, the standard deviation of phase-disordered results shows a peak at $\lambda = 0.4$ and $\lambda = 0.3$ for scenarios 5 and 9 and respectively 1. Phase-ordered results show now trivial behavior, with decreasing tendency with the exception of scenario 9. Finally, it is important to notice that R_{uni} captures the difference in modeling the coupling strength. Scenario 5, representing the unique thermal capacity of the lines shows a steep increase as the function of λ , showing that a heterogeneous grid structure tends to desynchronize under less severely weakened states.

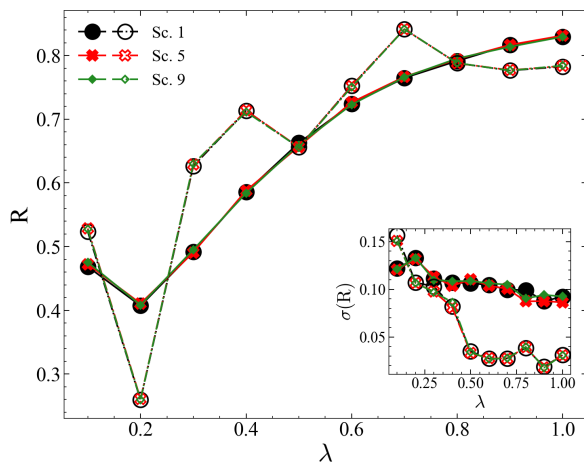


FIG. 1. Main figure: the Kuramoto order parameter R in the steady state, defined by Eq. (5) as the function of different λ values for scenarios 1, 5 and 9. Inset: the corresponding standard deviations of the Kuramoto order parameter, $\sigma(R)$.

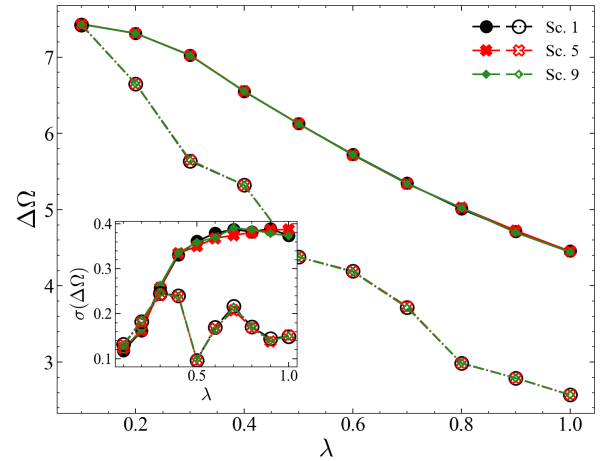


FIG. 2. Main figure: Frequency spread measured in the steady state, defined by Eq. (6), across various λ values. Note that $\Delta\Omega$ means the deviation compared to the nominal Ω_i . Inset: standard deviation of the frequency spread.

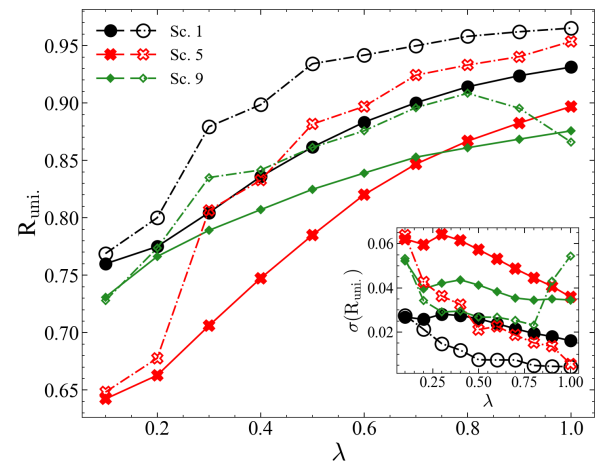


FIG. 3. Main figure: the universal order parameter, R_{uni} , in the steady state, defined by Eq. (8). Inset: standard deviation of R_{uni} , as the function of different λ values.

B. Kuramoto order parameter transient behavior

Fig. 4 shows the Kuramoto order parameter, R in the transient from different initial conditions. It can be seen that the scenarios align in three curves. The highest R values are reached by scenarios 1, 5, and 9 ($R \approx 0.7$ for phase disordered initial conditions), then 2, 6, and 10 ($R \approx 0.5$), and finally by 3, 7, and 11 ($R \approx 0.4$). These results indicate that changing the coupling strength, W_{ij} does not cause visible changes in steady-state values of R if all other parameters are fixed. This implies that R is unable to describe the synchronization behavior by changing the characteristics of the transmission lines. It can also be seen that increasing the heterogeneity of the moment of inertia, M_i , decreases the value of the order parameter,

as expected.

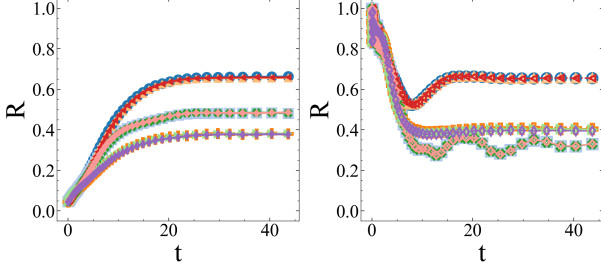


FIG. 4. Kuramoto order parameter, R for phase disordered (left) and for phase ordered initial conditions (right) at $\lambda = 0.5$. Scenarios 4, 8, and 12 are not displayed due to very low synchronization. Filled symbols: unordered initial conditions, empty ones ordered initial conditions. The blue circle denotes Scenario 1, light blue squares 2, orange plus 3, light orange triangle up 5, green X 6, light green triangle right 7, red triangle left 9, light red diamond 10, purple thin diamond is 11. The same markers and styling apply to Figs.5 and 6.

C. The Ω order parameter transient

Fig. 5 shows the evolution of the order parameter Ω . Similarly to the results of R , the scenarios form three distinct curves. However, the order of these curves is the opposite of the Kuramoto order parameter. Scenarios 1, 5, and 9 exhibit the lowest results ($\Delta\Omega \approx 6$ for phase disordered initial conditions), followed by 2, 6, and 10 ($\Delta\Omega \approx 40$), and by 3, 7, and 11 ($\Delta\Omega \approx 5000$). These results again imply that changing the coupling strengths, W_{ij} does not affect the steady-state values of Ω too much if all other parameters are fixed, thus heterogeneity in the edge behavior seems to be irrelevant.

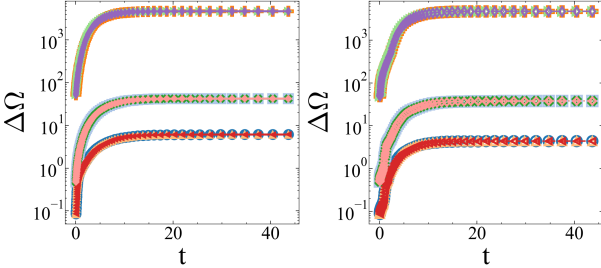


FIG. 5. Evolution of frequency spread Ω for phase disordered (left) and for phase ordered initial conditions (right) for $\lambda = 0.5$. Scenarios 4, 8, and 12 are not displayed due to very low synchronization. Symbols are the same as in Fig. 4.

D. The new order parameter R_{uni}

Fig. 6 shows the evolution of R_{uni} from disordered (left) and from ordered (right) initial conditions. This time all nine curves are separated, thus it is validated that R_{uni} is able to capture different heterogeneity of the model. Similarly to the

other order parameters, the highest synchronization is shown by the completely homogeneous model, Scenario 1. However, the results of the other scenarios are significantly different than before. In general, unique nodal behavior modeled through L_i and M_i decreases synchronization, which is an important advantage compared to the use of R , shown in Section III B.

When comparing the scenarios, an interesting behavior can be observed. If only the heterogeneity of the coupling strength, W_{ij} is increased, better synchronization is found in the case of the scenarios, where the values of W_{ij} are calculated from admittances (Scenarios 9, 10, 11) as compared to the ones, where actual thermal capacity was considered (5, 6, 7). If we compare curves with the same coupling strength, it is seen that the benchmark of literature, namely assuming the moment of inertia of a large power plant at each node, is a significant factor in reaching high synchronization. (E.g. $R_{uni} \approx 0.9$ for Scenario 1 and ≈ 0.8 for Scenario 2.) However such models are demonstrably overly optimistic, especially with the increase of non-synchronous generation in the mix³⁹. As R_{uni} is able to capture the different nodal behaviors and also shows their dependency on the coupling strength, its use over R should be favored, especially when using the Kuramoto model for grid case studies.

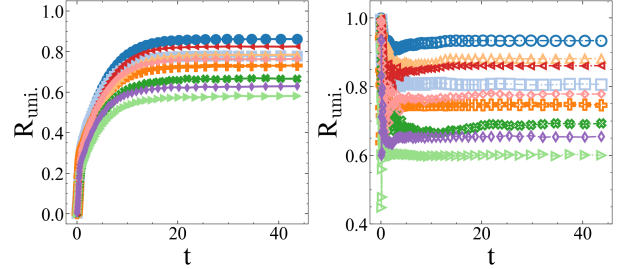


FIG. 6. Evolution of R_{uni} for phase disordered (left) and for phase ordered initial conditions (right) at $\lambda = 0.5$. Scenarios 4, 8, and 12 are not displayed due to very low synchronization. Symbols are the same as in Fig. 4.

E. Frequency distributions

Testing the predictive power of the Kuramoto-based modeling is a great challenge and has not been done on the quantitative level on realistic power-grids, according to our knowledge. Here we show node frequency results obtained by different levels of parameter approximations. We calculated the PDF-s at nodes obtained in the steady state form samples at the last 10 time steps and from thousands of independent realizations, which differ in the input/output power by the addition of the small quenched fluctuation values as shown in Eq.(3).

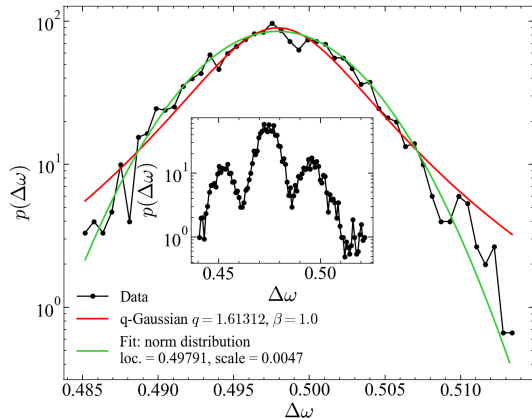


FIG. 7. Local frequency fluctuation distributions with respect to Ω_i , obtained for Scenario 9, corresponding to Békéscsaba substation for $\lambda = 0.5$ with different numerical fits. The best fit is obtained with the Student's t-distribution. The q-Gaussian provides $q \simeq 1.61$, close to the measurements. This particular node was chosen, because real data was fitted for the same substation in one of our previous works²⁰. Similar distribution results were obtained for the other substations (e.g. Detk, Győr) as well. The inset shows the typical multi-peak behavior in the case of $\lambda \neq \lambda_c$ at the same node, in the present case, for $\lambda = 0.6$.

These calculations were done for each scenario and for each λ . We tried to fit the PDF-s with the 8 most popular distributions: Gaussian, exponential, Student's t, log-normal, Pareto, double Weibull, generalized extreme value, and beta, from the Python distfit package as well as by the q-Gaussian functions as this distribution was commonly fitted well other HV studies of AC electrical data^{20,40}. Agreement with the q-Gaussian is remarkably good for lower λ values, see Fig 7 in case of Scenario 9.

For $\lambda > \lambda_c$ we found multi-peak behavior as displayed on the inset of Fig. 7 even though the width of the frequency spread decreases by increasing λ . Multi-peak frequency behavior is very common in the European power grid, especially in islands, like Great Britain, Ireland, and Mallorca.^{41,42} A numerical analysis based on the extension of the swing equations with a time-dependent damping factor could reproduce such global frequency fluctuations, suggesting that the system is wandering around the nominal 50Hz peak⁴².

Our swing equation solutions on the full Hungarian power-grid network suggest that even with constant parameters multi-peak frequency behavior can emerge when we overload the system with global power transmission above the synchronization point λ_c . Thus, beyond temporally different behavior we can also find sub-peaks on static power grids, due to the network heterogeneity. Note, that in our previous large-scale simulations, we showed different synchronization behaviors at fixed control parameters in different communities of Europe^{20,43}. This may hint at the dangers in power grids with multi-peaks being out of optimal operation control even if the frequency spread is narrow.

For scenarios other than 9 fat-tailed distributions were also

obtained. As they are very numerous publication of them will be published elsewhere.

IV. DISCUSSION AND CONCLUSIONS

As it was shown in the comparative analysis of Section III, the use of R_{uni} , proposed by Ref.²⁶ is encouraged to display the differences of heterogeneous power grid models. We found that in contrast to R and Ω , this order parameter is able to capture the difference of the coupling strength, showing higher synchronization values when W_{ij} is calculated based on the admittances of power lines. We also found that decreasing inertia of the system is more distinctly presented across the different scenarios. This feature of R_{uni} is especially advantageous for case studies, as the benchmark models of the literature tend to overestimate the amount of inertia in the system.

Considering the modeling depth, we found that completely heterogeneous models with unique nodal behavior based on SCADA measurements show very low synchronization and thus seem to be inappropriate for Kuramoto models. The underlying reasons could be (i) the ignorance of power losses and (ii) the ignorance of reactive power. To bridge these gaps, a promising approach was presented in Refs.^{28,38}, where the voltage magnitudes are incorporated in the Kuramoto model.

We provided local frequency results for the whole Hungarian power-grids, agreeing quite well with empirical measurements²⁰. The calculated PDF-s of $\Delta\Omega$, with respect to the nominal 50 Hz exhibit similar width and shapes as those recorded and published in²⁰. For λ -s, which drive the system above the synchronization point earlier we observed community dependent synchronization^{20,43}. These are related to the frequency multi-peaks of static models we report now. This means, that they occur not only in systems with time dependent parameters, but spatial heterogeneity can also induce them and warn for over-driven power grids, in the sense that they are away from the optimal SOC behavior.

ACKNOWLEDGMENTS

Bálint Hartmann acknowledges the support of the Bolyai János Research Scholarship of the Hungarian Academy of Sciences. Support from the Hungarian National Research, Development and Innovation Office NKFIH (K146736) is also acknowledged.

DATA AVAILABILITY STATEMENT

The data that support the findings of this study are available from the corresponding author upon reasonable request.

REFERENCES

- 1A. Somasekhar, M. Parraga, and C. Williams, “Texas power outages hinder Hurricane Beryl recovery, delay oil infrastructure restarts,” <https://www.reuters.com/world/us/power-outages-hinder-hurricane-beryl-recovery-delay-port-infrastructure-restarts-2024-07-10/> (2024), accessed: 29-08-2024.
- 2P. Milic, “A major power outage hits balkan region as countries swelter in an early summer heat wave,” <https://apnews.com/article/balkans-heat-wave-warnings-72b80a830b8bb275f377818ab2e41076> (2024), accessed: 29-08-2024.
- 3C. Graham-McLay, “Much of New Zealand’s far north is without power after a transmission tower fell over,” <https://apnews.com/article/fallen-tower-power-zealand-transmission-electricity-outage-northland-40f416a3cdaa67209eccf77cc4568382> (2024), accessed: 29-08-2024.
- 4S. Whiting, “Mass Bay Area power outages still affecting 200,000 PG&E customers,” <https://www.sfchronicle.com/bayarea/article/pge-outages-california-storms-wind-rain-17839576.php> (2024), accessed: 29-08-2024.
- 5S. Saifi, A. Syed, and R. Mogul, “Nearly 220 million people in Pakistan without power after countrywide outage,” <https://edition.cnn.com/2023/01/22/asia/pakistan-power-outage-intl-hnk/index.html> (2023), accessed: 29-08-2024.
- 6B. A. Carreras, D. E. Newman, I. Dobson, and A. B. Poole, “Evidence for self-organized criticality in a time series of electric power system blackouts,” *IEEE Trans. Circuits Syst. I: Regul. Pap.* **51**, 1733–1740 (2004).
- 7I. Dobson, B. A. Carreras, V. E. Lynch, and D. E. Newman, “Complex systems analysis of series of blackouts: Cascading failure, critical points, and self-organization,” *Chaos* **17**, 026103 (2007).
- 8G. Filatrella, A. H. Nielsen, and N. F. Pedersen, “Analysis of a power grid using a kuramoto-like model,” *Eur. Phys. J. B* **61**, 485–491 (2008).
- 9G. Ódor and B. Hartmann, “Heterogeneity effects in power grid network models,” *Physical Review E* **98**, 022305 (2018).
- 10G. Ódor and B. Hartmann, “Power-law distributions of dynamic cascade failures in power-grid models,” *Entropy* **22**, 666 (2020).
- 11G. Ódor, S. Deng, B. Hartmann, and J. Kelling, “Synchronization dynamics on power grids in europe and the united states,” *Phys. Rev. E* **106**, 034311 (2022).
- 12J. E. Cohen and P. Horowitz, “Paradoxical behaviour of mechanical and electrical networks,” *Nature* **352**, 699 (1991).
- 13D. Witthaut and M. Timme, “Braess’s Paradox in Oscillator Networks, Desynchronization and Power Outage,” *New Journal of Physics* **14**, 083036 (2012).
- 14D. Witthaut and M. Timme, “Nonlocal failures in complex supply networks by single link additions,” *The European Physical Journal B* **86**, 1–12 (2013).
- 15M. Fazlyaba, F. Dörfler, and V. M. Preciado, “Optimal network design for synchronization of kuramoto oscillators,” *arXiv preprint:1503.07254v2* (2015).
- 16L. S. Nagurny and A. Nagurny, “Observation of the braess paradox in electric circuits,” *Europhysics Letters* **115**, 28004 (2016).
- 17T. Coletta and P. Jacquod, “Linear stability and the braess paradox in coupled-oscillator networks and electric power grids,” *Physical Review E* **93**, 032222 (2016).
- 18A. E. Motter and M. Timme, “Antagonistic phenomena in network dynamics,” *Annual Review of Condensed Matter Physics* **9**, 463–484 (2018).
- 19G. Ódor, I. Papp, K. Benedek, and B. Hartmann, “Improving power-grid systems via topological changes or how self-organized criticality can help power grids,” *Phys. Rev. Res.* **6**, 013194 (2024).
- 20B. Hartmann, G. Ódor, I. Papp, K. Benedek, S. Deng, and J. Kelling, “Dynamical heterogeneity and universality of power-grids,” *Sustainable Energy, Grids and Networks* **39**, 101491 (2024).
- 21L. Schimansky-Geier, “Kuramoto, y., chemical oscillations, waves, and turbulence. berlin-heidelberg-new york-tokyo, springer-verlag 1984. viii, 156 s., 41 abb., dm 79,—. us \$ 28.80. isbn 3-540-13322-4 (springer series in synergetics 19),” *ZAMM - Journal of Applied Mathematics and Mechanics / Zeitschrift für Angewandte Mathematik und Mechanik* **66**, 296–296 (1986), <https://onlinelibrary.wiley.com/doi/pdf/10.1002/zamm.19860660706>.
- 22S. H. Strogatz, “From kuramoto to crawford: exploring the onset of synchronization in populations of coupled oscillators,” *Physica D: Nonlinear Phenomena* **143**, 1–20 (2000).
- 23A. Arenas, A. Díaz-Guilera, J. Kurths, Y. Moreno, and C. Zhou, “Synchronization in complex networks,” *Phys. Rep.* **469**, 93–153 (2008).
- 24S. Boccaletti, V. Latora, Y. Moreno, M. Chavez, and D.-U. Hwang, “Complex networks: Structure and dynamics,” *Physics Reports* **424**, 175–308 (2006).
- 25J. Gómez-Gardeñes, Y. Moreno, and A. Arenas, “Paths to synchronization on complex networks,” *Phys. Rev. Lett.* **98**, 034101 (2007).
- 26M. Schröder, M. Timme, and D. Witthaut, “A universal order parameter for synchrony in networks of limit cycle oscillators,” *Chaos* **27**, 073119 (2017).
- 27J. Grainger, J. and D. Stevenson, W., *Power system analysis* (McGraw-Hill, 1994).
- 28H. Taher, S. Olmi, and E. Schöll, “Enhancing power grid synchronization and stability through time-delayed feedback control,” *Physical Review E* **100** (2019), 10.1103/physreve.100.062306.
- 29S. Olmi, “The kuramoto model with inertia: from fireflies to power grids,” School and Workshop on Patterns of Synchrony: Chimera States and Beyond (July).
- 30P. Menck, J. Heitzig, J. Kurths, and H. Schellnhuber, “How dead ends undermine power grid stability,” *Nature communications* **5**, 3969 (2014).
- 31M. E. J. Newman, “Modularity and community structure in networks,” *Proc Natl Acad Sci U S A* **103**, 8577–8582 (2006).
- 32A. Fronczak, P. Fronczak, and J. A. Hołyst, “Average path length in random networks,” *Phys. Rev. E* **70**, 056110 (2004).
- 33Q. K. Telesford, K. E. Joyce, S. Hayasaka, J. H. Burdette, and P. J. Laurienti, “The ubiquity of small-world networks,” *Brain Connectivity* **1**, 367–375 (2011), PMID: 22432451.
- 34V. Latora and M. Marchiori, “Efficient behavior of small-world networks,” *Phys. Rev. Lett.* **87**, 198701 (2001).
- 35R. V. Solé, M. Rosas-Casals, B. Corominas-Murtra, and S. Valverde, “Robustness of the european power grids under intentional attack,” *Phys. Rev. E* **77**, 026102 (2008).
- 36P. Bak, C. Tang, and K. Wiesenfeld, “Self-organized criticality: An explanation of the 1/f noise,” *Phys. Rev. Lett.* **59**, 381–384 (1987).
- 37I. Dobson, B. A. Carreras, V. E. Lynch, and D. E. Newman, “Complex systems analysis of series of blackouts: Cascading failure, critical points, and self-organization,” *Chaos* **17**, 026103 (2007).
- 38K. Schmietendorf, J. Peinke, R. Friedrich, and O. Kamps, “Self-organized synchronization and voltage stability in networks of synchronous machines,” *The European Physical Journal Special Topics* **223**, 2577–2592 (2014).
- 39B. Hartmann, I. Vokony, and I. Táció, “Effects of decreasing synchronous inertia on power system dynamics—overview of recent experiences and marketisation of services,” *International Transactions on Electrical Energy Systems* **29** (2019), 10.1002/2050-7038.12128.
- 40B. Schäfer, C. Grabow, S. Auer, J. Kurths, D. Witthaut, and M. Timme, “Taming instabilities in power grid networks by decentralized control,” *The European Physical Journal Special Topics* **225**, 569–582 (2016).
- 41J. Kruse, B. Schafer, and D. Witthaut, “Predictability of power grid frequency,” *IEEE Access* **8**, 149435–149446 (2020).
- 42D. Kraljic, “Towards realistic statistical models of the grid frequency,” *IEEE Transactions on Power Systems* **38**, 256–266 (2023).
- 43S. Deng and G. Ódor, “Chimera-like states in neural networks and power systems,” *Chaos: An Interdisciplinary Journal of Nonlinear Science* **34** (2024), 10.1063/5.0154581.